Convergent Energies and Anharmonic Vibrational Spectra of Ca_2H_2 and Ca_2H_4 Constitutional Isomers

Journal:	*Physical Chemistry Chemical Physics*
Manuscript ID	CP-ART-03-2019-001643.R1
Article Type:	Paper
Date Submitted by the Author:	23-Apr-2019
Complete List of Authors:	Bowman, Michael; University of Georgia, Center for Computational Quantum Chemistry Gary, Douberly; University of Georgia, Department of Chemistry Schaefer, Henry; University of Georgia, Computational Chemistry

Journal Name

ARTICLE TYPE

Cite this: DOI: 10.1039/xxxxxxxxxx

Convergent Energies and Anharmonic Vibrational Spectra of Ca_2H_2 and Ca_2H_4 Constitutional Isomers†

Michael C. Bowman,[a] Gary E. Douberly,[b] and Henry F. Schaefer III*[a]

Received Date
Accepted Date

DOI: 10.1039/xxxxxxxxxx

www.rsc.org/journalname

Three constitutional isomers of both Ca_2H_2 and Ca_2H_4 have been characterized with molecular electronic structure theory. Correlation methods as complete as CCSDT(Q) and basis sets as large as cc-pwCV5Z have been used to converge the relative energies within chemical accuracy ($\leq$ 1 kcal mol^{-1}). Anharmonic vibrational frequencies were computed using second-order vibrational perturbation theory employing CCSD(T)/cc-pwCVTZ cubic and quartic force-fields and a CCSD(T)/cc-pwCVQZ quadratic force field. The monobridged [Ca(μ_2−H)CaH] and dibridged [Ca(μ_2−H)$_2$Ca] isomers of Ca_2H_2 were predicted to lie 6.5 and 12.9 kcal mol^{-1} below the energy of the classical HCaCaH linear isomer, respectively. Despite the energetic favorability of the bridged Ca_2H_2 isomers, we conclude (surprisingly) that only the higher energy linear structure has been observed in the laboratory. At 0 K, the tribridged [Ca(μ_2−H)$_3$CaH] isomer of Ca_2H_4 is predicted to be enthalpically favored by 0.9 kcal mol^{-1} in comparison to the enthalpy of the dibridged [HCa(μ_2−H)$_2$CaH] structure. Comparison of experiment with our computed frequencies suggests that the observed vibrational features arise from both the dibridged *and* the tribridged Ca_2H_4 structures.

1 Introduction

Mukherjee, Schuhknecht, and Okuda have reviewed recently the rapidly expanding field of molecular calcium hydrides[1]. Molecular calcium hydrides have a strong affinity to dimerize, forming (L)Ca(μ_2-H)$_2$Ca(L) complexes.[2,3] These dimeric calcium hydrido complexes serve as efficient catalysts for various reactions including hydrogenation[4,5], hydroboration[6,7], and hydrosilylation[8]. Solid calcium hydride $[CaH_2]_\infty$ has also been the subject of many studies due to its potential use as a doping agent for hydrogen storage materials.[9–11] While great attention has been given to calcium hydrido complexes in solution and calcium hydride in the solid state, less is known about calcium hydride systems in the gas phase.

In 1991, Xiao, Hauge, and Margrave performed the first FTIR matrix isolation spectroscopic study of the reaction of photoexcited calcium with an excess of H_2.[12] By adjusting the photolysis source and vaporization temperature and by replacing the hydrogen with isotopologues, these authors assigned peaks to the CaH_2, Ca_2H_2, and Ca_2H_4 molecules in krypton and xenon matrices. Later, in 2004, Wang and Andrews performed a related study in solid neon, argon, and hydrogen, but used laser ablation as the calcium source instead of vaporization. These authors made similar assignments for CaH_2, Ca_2H_2, and Ca_2H_4.[13] To our knowledge, Ca_2H_2 and Ca_2H_4 have not been detected in the gas phase. In the present study, we interpret the previous matrix isolation experiments as well as make predictions for how Ca_2H_2 and Ca_2H_4 might be characterized in the gas phase.

As a fourth row element, calcium falls between the lighter alkaline earth metals (Be and Mg) and the heavier metals (Sr and Ba) in terms of polarizability. Calcium's intermediate degree of polarizability makes it difficult to predict *a priori* whether it will behave like its lighter or heavier congeners. For example, many theoretical studies have predicted that CaH_2 should be linear like MgH_2 and BeH_2 instead of bent like SrH_2 and BaH_2.[14–16] However, infrared spectra from Xiao et al and from Wang and Andrews both suggested that CaH_2 was quasilinear.[12,13] This observation was later corroborated by Koput, who used CCSD(T) with quadruple- and quintuple-ζ basis sets to obtain equilibrium bond angles of 167.1° and 164.4°, respectively.[17] The success of coupled cluster methods with large basis sets, over lower levels of theory, in correctly predicting the quasilinearity of CaH_2 demonstrated the necessity for high level *ab initio* characterization for calcium hydride species.

Ab initio studies on M_2H_2 (M = Be, Mg, Ca, Sr, or Ba) alkaline earth metal hydrides have explored local minima corresponding to both linear [HMMH] and bridged [M(μ_2-H)MH or M(μ_2-

[a] *Center for Computational Quantum Chemistry, University of Georgia, Athens, Georgia. Email: ccq@uga.edu*
[b] *Department of Chemistry, University of Georgia, Athens, Georgia*

† Electronic Supplementary Information (ESI) available: [Geometries, vibrational frequencies, electronic energies, dipole moments, multireference diagnostics, relaxed potential surface scans, QSD reaction paths, etc]. See DOI:

$H)_2M$] structures.[18–20] For the lighter metal hydrides Be_2H_2 and Mg_2H_2 the linear structure was favored over the bridged structures.[19,21–23] On the other hand the heavier metal hydrides Sr_2H_2 and Ba_2H_2 have a preference for bridged or branched (e.g. $BaBaH_2$) structures.[13] In 2003, Magnusson and Petrie examined many M_2H_2 species at the B3LYP and G2 levels of theory and concluded that Ca_2H_2 was similar to its heavier congeners in its preference for bridged structures.[24] However, despite the thermodynamical favorability of the monobridged and dibridged Ca_2H_2 structures, only the linear Ca_2H_2 structure has been experimentally examined.

Dimerization of MH_2 monomers yields M_2H_4 hydrides. Kaupp and Schleyer[25] determined that the factors controlling the monomeric MH_2 bond angle, namely the polarizability of the alkaline metal and d orbital participation in σ-bonding, were also responsible for the bridging preferences in M_2H_4 hydrides. Theoretical and experimental studies alike have shown that Be_2H_4 and Mg_2H_4 possess a dibridged [$HM(\mu_2\text{-}H)_2MH$] D_{2h} geometry as a global minimum.[18,23,26] Contrarily, Sr_2H_4 and Ba_2H_4 preferentially form tribridged C_{3v} structures [$HM(\mu_2\text{-}H)_3M$].[13,25] Once again calcium represents an intermediate case between the lighter and heavier alkaline earth metals. MP2 studies performed by Kaupp and Schleyer[25] in 1993 reported that the dibridged structure was preferred over the tribridged by 1.4 kcal mol^{-1}. However, Wang and Andrews later computed the tribridged Ca_2H_4 structure to be lower in energy by 1.2 kcal mol^{-1} at the B3LYP/6-311++G(3df,3pd) level of theory.[13] Wang and Andrews also computed B3LYP harmonic vibrational frequencies for both the dibridged and tribridged Ca_2H_4 isomers, but were unable to confidently determine which isomer was responsible for the Ca_2H_4 bands observed. Given the above modest theoretical treatments, it is currently unclear whether the dibridged or the tribridged Ca_2H_4 structure is the lowest energy constitutional isomer and which structure has been observed in the various matrices.

In the present study, we have performed a high-level *ab initio* characterization of minima and transition states on the Ca_2H_2 and Ca_2H_4 potential energy surfaces to confidently determine the relative enthalpies of calcium hydride species at 0 K. Additionally, we have computed fundamental frequencies for Ca_2H_2 and Ca_2H_4 species to aid the spectroscopic identification of calcium hydrides.

2 Methods

Coupled cluster theory with single, double, and perturbative triple excitations [CCSD(T)][27] was used to characterize stationary points on the Ca_2H_2 and Ca_2H_4 surfaces. Contributions from calcium's outer-core ($3s^23p^6$) shell were considered through the use of cc-pwCVXZ (X = D, T, Q, 5) basis sets[28] and by freezing only the ten inner most electrons ($1s^22s^22p^6$) on each calcium atom. Diffuse basis functions (i.e. aug-cc-pVXZ) were added to the relatively electronegative hydrogen atoms to account for the expected negative charge on these atoms[29]. For brevity we will use "XZ" to denote the use of cc-pwCVXZ on calcium atoms and aug-cc-pVXZ on the hydrogen atoms. Preliminary results confirmed that this choice of basis set and electron correlation provided results that converged to experimental values for calcium monohydride (CaH $^2\Sigma^+$). The methods used in this study are also consistent with recent high-level *ab initio* studies performed on the related molecules CaH and CaH_2.[17,30–32]

Equilibrium geometries were optimized at the CCSD(T)/QZ level of theory to a RMS energy gradient of 1.0×10^{-7}. Harmonic vibrational frequencies were obtained for the CCSD(T)/QZ optimized geometries at the same level of theory. The harmonic vibrational frequencies were used to characterize stationary points as minima or transition states. Equilibrium geometries and harmonic vibrational frequencies were obtained using the MOLPRO 2010 package.[33] The connections between transition states and minima were verified using Quadratic Steepest Descent Reaction Path Following[34,35] as implemented in MOLPRO 2010 at the CCSD(T)/DZ level of theory. Full cubic and semidiagonal quartic anharmonic contributions to the vibrational frequencies were computed for local minima at the CCSD(T)/TZ level of theory with second order vibrational perturbation theory (VPT2)[36] as implemented in CFOUR 2.0.[37] The anharmonic contributions were appended to the harmonic vibrational frequencies obtained at the CCSD(T)/QZ level of theory to predict the fundamental frequencies. Additionally, the dipole moments of CaH, $HCa(\mu_2\text{-}H)Ca$ and $HCa(\mu_2\text{-}H)_3Ca$ were computed at the CCSD/QZ level of theory.

The electronic energies of stationary points were computed according to the focal point analysis (FPA) of Allen and coworkers.[38–41] Electron correlation treatments up to CCSDT(Q) and basis sets as large as quintuple-ζ (i.e. 5Z) were used in this study. Complete basis set (CBS) energies were obtained for various methods by extrapolating the Hartree-Fock reference energies and correlation energies using a three-point exponential equation[42] and a two-point inverse cubic equation[43], respectively:

$$E_{\mathrm{ref}}(X) = E_{\mathrm{ref}}^{\infty} + ae^{-bX} \quad (1)$$

$$E_{\mathrm{corr}}(X) = E_{\mathrm{corr}}^{\infty} + aX^{-3} \quad (2)$$

The CCSDT(Q)/CBS energy was determined by appending CCSDT(Q) and CCSDT additive corrections to the CCSD(T)/CBS energy. The CCSDT(Q) and CCSDT corrections were computed with the MRCC 2015[44] package using DZ and TZ basis sets, respectively. The CCSDT and CCSDT(Q) corrections are reported as a single higher order correlation correction ($\delta_{\mathrm{T(Q)}}$). Further corrections were included to account for the limitations of approximations used to compute the CCSDT(Q)/CBS energy. The impact of calcium's inner-core-correlation was accounted for by a CCSD(T)/QZ all-electron computation. Scalar relativistic effects were considered using second-order direct perturbation theory (DPT2)[45] at the CCSD(T)/TZ level of theory with all the electrons correlated. The correction for the inner-core correlation and the scalar relativistic correction largely cancel each other out, therefore we list only the combined correction (δ_{CR}). An adiabatic diagonal Born-Oppenheimer correction (δ_{DBOC})[46,47] was performed at the HF/QZ level of theory to account for the clamped-nuclei approximation. Finally, the harmonic zero-point vibrational energy (δ_{ZPVE}) was appended to determine the relative enthalpy at zero Kelvin (ΔH_{0K}). The matrix isolation studies have been performed at temperatures less than 15K; there-

fore it was unnecessary to compute thermal corrections in order to accurately interpret the experimental results. Nevertheless, in order to predict the equilibrium constant between the dibridged and tribridged Ca_2H_4 structures at higher temperatures we have calculated the relative Gibbs free energy ($\Delta G(T)$) for these constitutional isomers using a rigid-rotor harmonic-oscillator partition function.

3 Results and Discussion

3.1 Ca_2, CaH, and CaH_2

A plethora of theoretical and experimental research has been reported on the calcium dimer, calcium monohydride, and calcium dihydride. These results provide us with ample comparisons to validate our theoretical methods.

The alkaline earth metals have been shown in several studies to form weakly-bound van der Waals dimers.[48–52] Francis and Weber[53] observed that calcium has an affinity to aggregate into Ca_2 dimers when deposited into solid krypton; therefore it is likely that Ca_2 was initially present in the matrix isolation experiments of Xiao et al[12] and Wang and Andrews[23]. However, the calcium dimer is a particularly difficult system to model because of its shallow potential well. Table 1 compares our Ca_2 results to experimental and previous theoretical results. Many studies have employed augmented basis sets to model the weak Ca–Ca interaction; however, by comparing the results we obtained using CCSD(T)/cc-pwCVQZ to the results Yang and Wang obtained with CCSD(T)/aug-cc-pCVQZ, we find the addition of diffuse functions has a negligible effect on the molecular properties of Ca_2. On the other hand, incorporation of corrections for iterative triple and perturbative quadruple amplitudes [i.e. CCSDT(Q)] into the CCSD(T) geometry optimization decreases the equilibrium Ca–Ca distance by about 0.05 Å, bringing it into better agreement with experiment. However, we expect the incorporation of quadruple excitations to have a significantly decreased effect on the equilibrium geometries of calcium hydrides. Hence, the error within our Ca_2 theoretical results can be viewed as an upper-bound for the error elsewhere in this study.

Calcium monohydride is an important astronomical radical, as such it has received significant treatment both experimentally and theoretically. Table 2 shows our results for ground state CaH ($^2\Sigma^+$) in comparison to previous theoretical and experimental studies. At the CCSD(T)/QZ level of theory we were able to closely replicate the experimentally observed values for r_e, D_e, ω_e, and μ. This suggests that CCSD(T)/QZ is sufficient to make accurate predictions on the calcium hydrides within this study.

As mentioned in the introduction, the quasilinearity of CaH_2 long evaded a proper theoretical treatment. Table 3 lists the equilibrium geometry and fundamental vibrational frequencies of CaH_2 as observed in matrix isolation experiments and as predicted at various levels of theory. We find that our CCSD(T)/QZ optimization predicts CaH_2 to be slightly bent with an equilibrium bond angle of 166.0 degrees, which is in agreement with the prediction by Koput at the CCSD(T)/5Z level of theory[17] as well as the experimental conclusions made by Xiao et al[12] and by Wang and Andrews[13]. However, we found that at the CCSD(T)/TZ and

Table 1 Equilibrium bond distance (r_e, in Å), dissociation energy (D_e, in cm^{-1}), harmonic vibrational frequency (ω_e, in cm^{-1}) and anharmonicity constant ($\omega_e x_e$, in cm^{-1}) for the calcium dimer (Ca_2).

Work	r_e	D_e	ω_e	$\omega_e x_e$
CCSD(T)/QZ [a]	4.337	932	61.1	1.21
CCSDT(Q)/CBS [a]		990		
Experiment [b]	4.277	1075	64.9	1.07
Experiment [c]	4.276	1095	65.1	
Experiment [d]	4.277	1102	64.4	
CCSD(T)/aQZ [e]	4.339	930	61.3	1.15
CCSD(T)/a5Z [f]		983		
CCSDT(Q)/aCBS [e]	4.287	1095	63.8	1.15
CCSD(T)/GRECP [g]	4.283	1136	65.4	

[a] This research, $\omega_e x_e$ computed at the CCSD(T)/TZ level of theory
[b] Balfour and Whitlock[50]
[c] Vidal[54]
[d] Allard et al[55,56]
[e] Yang and Wang[57]
[f] Patwoski et al, all electron[58]
[g] Mosyagin et al[59]

Table 2 Equilibrium bond distance (r_e, in Å), dissociation energy (D_e, in cm^{-1}), harmonic vibrational frequency (ω_e, in cm^{-1}), anharmonicity constant ($\omega_e x_e$, in cm^{-1}), and dipole moment (μ in Debye) for calcium monohydride (CaH $^2\Sigma^+$).

Work	r_e	D_e	ω_e	$\omega_e x_e$	μ
CCSD(T)/QZ [a]	2.005	14410	1296.6	21.94	2.52
CCSDT(Q)/CBS [a]		14540			
Experiment [b]			1298.4	19.18	
Experiment [c]	2.003	14360	1298.3	19.10	2.50
MRCI+Q/QZ [e]	2.006	14330	1293.8	18.89	2.55
CCSD(T)/5Z [f]	2.004	14270			2.54

[a] This research, $\omega_e x_e$ computed at the CCSD(T)/TZ level of theory
[b] Petitprez et al[60]
[c] Huber and Herzberg[61]
[d] Chen and Steimle[62]
[e] Shayesteh et al[32]
[f] Kerkines and Mavridis[31]

Table 3 Equilibrium bond distance (r_e, in Å), bond angle (θ_e, in degrees), and fundamental frequencies (ν_i, in cm^{-1}) for CaH_2.

Work	r_e	θ_e	ν_1	ν_2	ν_3
CCSD(T)/QZ [a]	2.047	166.0	1295.7	91.2	1214.7
Experiment [b]		166(4)	1289.7		1216.3
Experiment [c]		168(4)	1267.0		1192.0
CCSD(T)/TZ [d]		180.0	1277.7	205.1	1195.8
CCSD(T)/5Z [e]	2.045	164.4	1298.5	116.1	1223.0

[a] This research
[b] Wang and Andrews, Ar matrix [13]
[c] Xiao et al, Kr matrix [12]
[d] Hrenar et al, VCI [63]
[e] Koput, VPT2 [17]

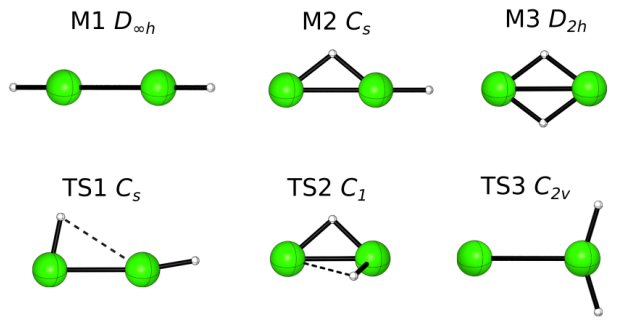

Fig. 1 Qualitative geometries of Ca_2H_2 stationary points. Bond lengths and angles are given in Table 4.

CCSD(T)/DZ level of theory CaH_2 had a linear structure as a minimum. Therefore, we propose basis sets of at least quadruple-ζ are necessary to confidently determine the qualitative geometry of calcium hydrides. Furthermore, when considering typical red-shifts associated with the Ar and Kr matrices, our VPT2 frequencies closely match the fundamental frequencies observed in both matrix isolation studies. Based on this, VPT2 with CCSD(T)/TZ cubic and semi-diagonal quartic force fields appears appropriate to predict calcium hydride gas-phase frequencies.

3.2 Ca_2H_2 Systems

Three equilibrium structures were optimized for the Ca_2H_2 calcium hydride: linear (M1), monobridged (M2), and dibridged (M3). The geometries of Ca_2H_2 stationary points are illustrated in Figure 1 and the relevant internal coordinates are provided in Table 4. The relative enthalpies of the Ca_2H_2 stationary points are calculated in Table 5 and illustrated in Figure 2. We have assumed that linear Ca_2H_2 (M1) is initially produced from the combination of two calcium monohydride radicals; however, the exact mechanism for Ca_2H_2 production is currently unclear.

All three constitutional isomers are thermodynamically favored over the dissociation products, 2 CaH, CaH_2 + Ca, or Ca_2 + H_2. Relaxed potential surface scans revealed the addition of 2 CaH → M1 and CaH_2 + Ca → M2 to proceed without an entrance barrier. On the other hand, it should be noted that the direct insertion of H_2 into Ca_2 is forbidden in C_{2v} symmetry on the ground state potential surface and will encounter a substantial entrance bar-

Table 4 Internal coordinates (in Å and degrees) for Ca_2H_2 species.

Species	Ca–Ca	Ca–H_t [a]	∠CaH_bCa [a]
M1 [HCaCaH]	3.733	2.024	
M2 [HCa(μ_2−H)Ca]	3.404	2.020	102.6
M3 [Ca(μ_2−H)$_2$Ca]	3.481		106.7
TS1 (M1→M2)	3.517	2.017	
TS2 (M2→M3)	3.183	2.012	94.9
TS3 (M2→M2)	4.049	2.051	

[a] H_t and H_b respectively indicate a terminal hydrogen and a bridging hydrogen.

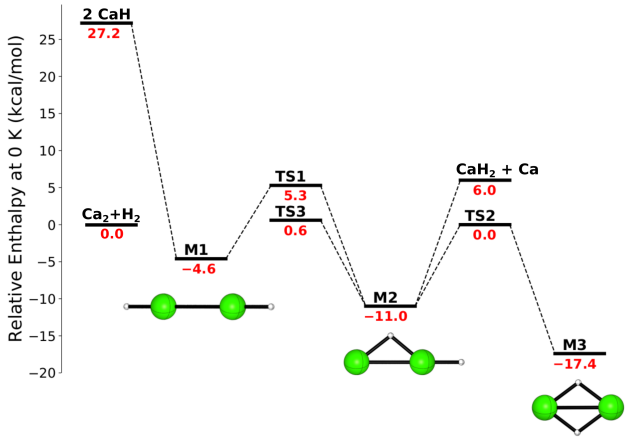

Fig. 2 Potential enthalpy diagram for Ca_2H_2 at 0 K. TS3 connects M2 to M2'.

Table 5 Enthaplies at 0 K (ΔH_{0K}) in kcal mol^{-1} of Ca_2H_2 species. CBS denotes the CCSD(T)/CBS relative energy. Delta (δ) denotes the change in relative energy with respect to the preceding level of theory or various additional corrections. See Methods section for details.

Species	CBS	$\delta_{T(Q)}$	δ_{CR}	δ_{DBOC}	δ_{ZPVE}	Total
2 CaH	28.93	0.16	0.82	0.15	−2.67	27.23
CaH_2 + Ca	8.20	0.32	−0.00	0.01	−2.56	5.97
TS1 (M1 → M2)	7.55	−0.11	−0.37	0.14	−2.24	5.27
TS2 (M2 → M3)	1.82	−0.19	−0.88	0.18	−0.93	0.01
TS3 (M2 → M2)	2.98	0.15	−0.36	0.10	−2.07	0.62
M1 [HCaCaH]	−2.92	0.10	−0.19	0.11	−1.67	−4.58
M2 [HCa(μ_2−H)Ca]	−9.36	−0.06	−0.68	0.14	−1.08	−11.04
M3 [Ca(μ_2−H)$_2$Ca]	−16.76	0.10	−1.33	0.36	0.20	−17.43
Ca_2 + H_2	0.00	0.00	0.00	0.00	0.00	0.00

rier. The dibridged structure is the lowest in enthalpy followed by the monobridged, then linear structures. As previously mentioned, this relative ordering is different than the isovalent Mg_2H_2 and Be_2H_2 isomers[19,20], but similar to the heavier alkaline earth metal hydrides Sr_2H_2 and Ba_2H_2[13]. The relative differences in enthalpies from monobridged to linear and from dibridged to monobridged are 6.5 and 6.4 kcal mol^{-1}, respectively. These may be compared with the results Magnusson and Petrie[24] obtained with the G2 method: 6.6 and 9.0 kcal mol^{-1}.

A C_{2v} branched ("vinylidene-like") geometry was also optimized for Ca_2H_2. The branched geometry lies 5.2 kcal mol^{-1} above the enthalpy of the linear Ca_2H_2 isomer, but 5.4 kcal mol^{-1} below the dissociation to CaH_2 + Ca. However, this stationary point features a symmetry breaking imaginary mode and was identified as the transition state (TS3) connecting similar monobridged structures. This is in contrast to the heavier alkaline earth metal hydrides Sr_2H_2 and Ba_2H_2, which both exhibit[13] branched minima with B3LYP.

At a photolysis wavelength of 580 nm, Xiao et al[12] observed a bright peak centered at 1237 cm^{-1} in a Kr matrix. By adjusting the H_2 pressure and Ca concentration as well as by replacing H_2 with isotopologues, these authors assigned the 1237 cm^{-1} peak to linear Ca_2H_2. In a similar manner, Wang and Andrews[13] observed a peak at 1240 cm^{-1} in their neon matrix and assigned it to linear Ca_2H_2. The fundamental frequencies and intensities of Ca_2H_2 minima are provided in Table 6. Our VPT2 analysis predicts a bright absorption band for the asymmetric Ca-H stretch in linear Ca_2H_2 at 1245 cm^{-1}. This result agrees well with the band observed in solid neon (1240 cm^{-1})[13] and krypton (1237 cm^{-1})[12], given the expected red-shift of the bands due to the neon and krypton matrices.

While both matrix isolation studies made assignments for the linear Ca_2H_2 asymmetric stretching frequency, neither study assigned frequencies to the lower in energy monobridged or dibridged Ca_2H_2 isomers. The monobridged structure has bright absorption bands at 1270 and 792 cm^{-1}, corresponding to the Ca-H stretch and Ca-H-Ca stretches, respectively. The most intense vibrational mode of the dibridged constitutional isomer is the Ca-H-Ca asymmetric stretch at 801 cm^{-1}, which is similar to the Ca-H-Ca stretch of the monobridged structure. While the 1270 cm^{-1} monobridged Ca-H stretch might coincide with the linear Ca_2H_2 asymmetric stretch, neither experimental study reported peaks in the 800-750 cm^{-1} region where the Ca-H-Ca stretching frequencies would occur. Therefore, the absence of a vibrational band around 800 cm^{-1} in both studies suggests that the monobridged and dibridged Ca_2H_2 isomers were not present in any matrix. This result is especially perplexing, because in related studies with isovalent magnesium hydride, the dibridged Mg_2H_2 structure was observed alongside the linear Mg_2H_2 structure even though the dibridged Mg_2H_2 structure is higher in energy.[22]

It is currently unclear how Ca_2H_2 is produced, but the lack of experimental observation (despite substantial predicted oscillator strength) of the bridged Ca_2H_2 calcium hydrides suggests that the linear Ca_2H_2 is initially produced and is kinetically hindered from converting to the enthalpically favored monobridged or dibridged structures. One possibility is that the photolysis source excites the calcium dimer to the $^1\Sigma_u^+$ or $^1\Pi_u$ state,[64] allowing the calcium dimer to react with H_2. An alternative mechanism would be two calcium monohydride monomers are initially formed from the photolysis of calcium in the matrix and recombine to produce Ca_2H_2. In either case, the excess internal energy released from the formation of linear Ca_2H_2 isomer would need to be quenched by the matrix before the linear structure isomerizes to a more favorable isomer. In Figure 2, we have assumed the latter to be the principle mechanism for Ca_2H_2 production. Transition states between Ca_2H_2 species were optimized in order to determine the feasibility of interconversion between these constitutional isomers. The barriers from the linear to monobridged structure (TS1) and from the monobridged to dibridged structure (TS2) were determined to be 9.9 and 11.0 kcal mol^{-1}, respectively. Given the moderate barrier to interconversion, it is plausible that the excess internal energy from the photolytic reaction of Ca_2 + H_2 → Ca_2H_2 dissipates into the surrounding matrix before the linear isomer can undergo interconversion to a more thermodynamically stable isomer. Nevertheless, it is conceivable that the monobridged and dibridged isomers could be produced within these matrices through tunneling of the hydrogen atoms. We suggest that future studies examine the timescales for tunneling between the linear isomer to the monobridged and dibridged structures.

The monobridged and dibridged structures are more likely to be produced in the gas phase, where the excess internal energy

Table 6 Fundamental vibrational frequencies of Ca_2H_2 species with anharmonic intensities. Frequencies are given in cm^{-1} and intensities are given in km mol^{-1}.

Species	Frequencies (Intensities)
M1 [HCaCaH]	1264 (σ_g, 0), 1245 (σ_u, 1684), 167 (π_g, 0 × 2),
linear	151 (σ_g, 0), 140 (π_u, 428 × 2)
M2 [HCa(μ_2−H)Ca]	1270 (a′, 742), 985 (a′, 17), 792 (a′, 832),
monobridged	220 (a′, 251), 159 (a′, 28), 144 (a″, 318)
M3 [Ca(μ_2−H)$_2$Ca]	1005 (b_{3u}, 41), 985 (a_g, 0), 956 (b_{1g}, 0),
dibridged	801 (b_{2u}, 123), 422 (b_{1u}, 5), 217 (a_g, 0)

would not be quenched as quickly. The monobridged structure has a a permanent dipole moment of 2.79 Debye units whereas the other Ca_2H_2 isomers do not have a dipole moment. Because the Ca-H-Ca stretching frequencies of the dibridged and monobridged isomer are very similar, microwave spectroscopy could be used to distinguish the monobridged Ca_2H_2 isomer from the dibridged isomer in the gas phase. We encourage future experimental characterizations of calcium hydride to attempt to observe monobridged and dibridged Ca_2H_2 in the gas phase.

3.3 Ca_2H_4 Systems

Three minima and transition states were optimized on the Ca_2H_4 surface: dibridged (M4, D_{2h}), tribridged (M5, C_{3v}), and tetrabridged (M6, D_{4h}). The geometries of Ca_2H_4 stationary points are depicted in Figure 3 and the relevant internal coordinates for Ca_2H_4 stationary points are given in Table 7. There is a clear trend in Table 7; as the number of bridging hydrogens is increased, the Ca–Ca bond distance and Ca-H-Ca bond angle both decrease. These trends can be intuitively assigned to the increased electrostatic attraction between calcium and hydrogen and increased electrostatic repulsion of bridging hydrogens, respectively. The relative enthalpies of these Ca_2H_4 stationary points are calculated in Table 8 and illustrated in Figure 4. We have assumed that dibridged Ca_2H_4 (M4) is directly produced from the dimerization of two CaH_2 monomers. Alternatively, tribridged Ca_2H_4 (M5) could also result from the dimerization of CaH_2, but a relaxed potential surface scan suggested that the direct production of dibridged Ca_2H_4 (M4) is more favorable. All three structures are bound with respect to dissociation to Ca_2 + 2 H_2 or two CaH_2 monomers, however the dibridged and tribridged isomers are significantly more thermodynamically favorable than the tetrabridged isomer.

In addition to the three Ca_2H_4 minima, we optimized a C_{2v} symmetric stationary point with two terminal hydrogens on the same calcium atom. This stationary point lies slightly above the energy of the tetrabridged Ca_2H_4 isomer, and is bound with respect to dissociation. In accord with the results of Kaupp and Schleyer[25], this stationary point has a symmetry breaking imaginary frequency leading to the tribridged isomer (M5). Thus the C_{2v} structure was identified as a transition state (TS6) directly connecting tribridged isomers.

Previous theoretical computations disagreed whether the dibridged or tribridged structure would be the global minimum. Table 9 shows a focal point comparison of the tribridged elec-

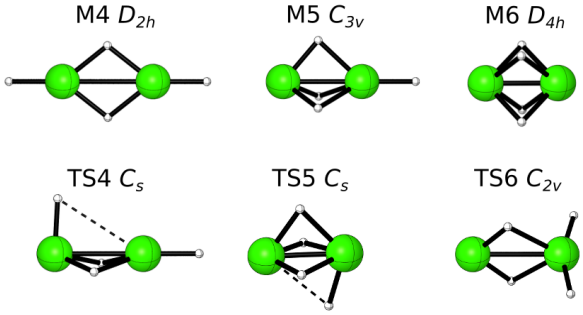

Fig. 3 Qualitative geometries of Ca_2H_4 stationary points. Bond lengths and angles are given in Table 7.

Table 7 Internal coordinates (in Å and degrees) for Ca_2H_4 species.

Species	Ca–Ca	Ca–H_t [a]	∠CaH_bCa [a]
M4 [HCa(μ_2−H)$_2$CaH]	3.438	2.032	103.3
M5 [Ca(μ_2−H)$_3$CaH]	3.006	2.048	86.7
M6 [Ca(μ_2−H)$_4$Ca]	2.655		75.4
TS4 (M4→M5)	3.233	2.034	96.4
TS5 (M5→M6)	2.753		78.9
TS6 (M5→M5)	3.323	2.093	97.6

[a] H_t and H_b respectively indicate a terminal hydrogen and a bridging hydrogen.

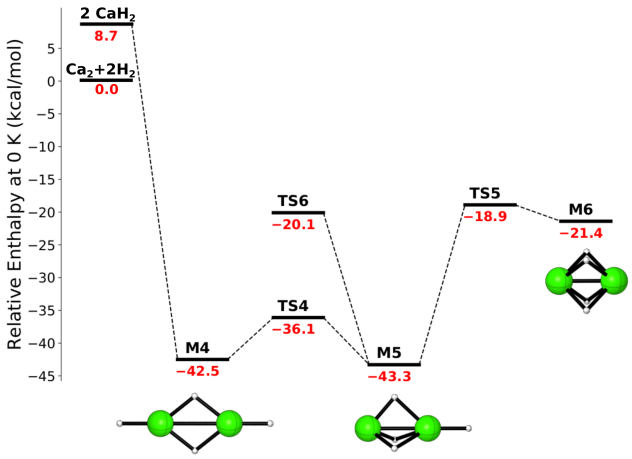

Fig. 4 Potential enthalpy diagram for Ca_2H_4 at 0K. TS6 connects M5 to M5'.

Table 8 Enthaplies at 0 K (ΔH_{0K}) in kcal mol^{-1} of Ca_2H_4 species. CBS denotes the CCSD(T)/CBS relative energy. Delta (δ) denotes the change in relative energy with respect to the preceding level of theory or various additional corrections. See Methods section for details.

Species	CBS	$\delta_{T(Q)}$	δ_{CR}	δ_{DBOC}	δ_{ZPVE}	Total
2 CaH_2	13.55	0.30	−0.33	0.18	−5.03	8.67
TS6 (M5 → M5)	−7.77	0.10	−1.82	0.20	−1.42	−10.72
TS5 (M5 → M6)	−16.63	−0.10	−2.40	0.23	0.34	−18.57
M6 [Ca(μ_2−H)$_4$Ca]	−19.95	−0.12	−2.48	0.24	0.90	−21.40
TS4 (M4 → M5)	−34.50	0.13	−1.88	0.20	−0.70	−36.76
M4 [HCa(μ_2−H)$_2$CaH]	−39.65	0.20	−2.08	0.20	−1.20	−42.54
M5 [HCa(μ_2−H)$_3$Ca]	−41.78	0.08	−2.14	0.21	0.29	−43.34
Ca_2 + 2 H_2	0.00	0.00	0.00	0.00	0.00	0.00

tronic energy relative to the dibridged electronic energy. At the CCSDT(Q)/DZ level of theory the dibridged structure is lower in energy. However, as we increase the size of the basis set the tribridged structure becomes increasingly more favorable. This trend is related to the increase in polarizability following the addition of basis functions. As the basis set is enlarged, the computed polarizability of the calcium atoms is increased[65], which lowers the energy of the tribridged and tetrabridged structures relative to the dibridged structure. By examining the incremental changes in energy in Table 9, we observe a tight convergence of the electronic energy to both the complete basis set (CBS) and full configuration interaction (FCI) limits. We can estimate the margin of error as the largest incremental correction (excluding δ_{ZPVE}) when calculating ΔH_{0K}. The largest correction comes from the extrapolation of the CCSD(T) energies to the complete basis set limit which is approximately 0.24 kcal mol^{-1}; thus we can be confident that the tribridged constitutional isomer is the lowest energy isomer at 0K.

While the tribridged isomer is enthalpically favored at low temperatures, it should be noted that the dibridged isomer has a larger ΔS. As the temperature is increased the Gibbs free energy [$\Delta G(T)$] between the tribridged and dibridged structure is reduced. Around 300 K, the dibridged structure has the more favorable ΔG, indicating that equilibrium will tend toward the dibridged isomer at moderate to high temperatures.

Dibridged Ca_2H_4 is principally formed from the barrierless dimerization of CaH_2 within the matrix. The interconversion of the dibridged to tribridged is hindered by an energetic barrier of 6.8 kcal mol^{-1} corresponding to TS4; however, this barrier is submerged significantly below the energy released from the dimerization of CaH_2 (51.6 kcal mol^{-1}). If the dissipation of internal energy to the matrix is slow relative to the rearrangement of vibrational energy within the molecule, then the Ca_2H_4 will be able to rearrange from the dibridged structure to the energetically favorable tribridged structure. On the other hand, if the matrix quickly dissipates the internal energy of Ca_2H_4, it would become kinetically trapped as the dibridged isomer. Since the dissipation rate is dependent on the polarizability of the matrix gas, it is more likely to observe the tribridged isomer in the lighter matrices such as neon and the dibridged isomer in heavier matrices such as krypton.

The fundamental vibrational frequencies of the Ca_2H_4 minima are provided in Table 10. Both matrix isolation infrared spectroscopy studies assigned several peaks to Ca_2H_4. However, previous authors were unable to differentiate whether these peaks arose from the dibridged or tribridged Ca_2H_4 isomers. Table 11 lists experimental frequencies assigned to Ca_2H_4 along with the most similar dibridged and tribridged fundamental frequency computed in this study. By comparing the neon, argon, and krypton frequencies, it appears the gas-phase fundamental frequencies are red-shifted with the increasing polarizability of the matrix environment. Peaks 1 and 2 can be confidently assigned to the tribridged structure, however, 3 and 4 are more accurately attributed to the tribridged structure. Furthermore, the 1258 cm^{-1} frequency of the tribridged isomer and the 1223 cm^{-1} frequency of the dibridged isomer overlap respectively with the CaH stretching frequency (1253 cm^{-1}) and the CaH_2 asymmetric stretching frequency (1215 cm^{-1}). The only Ca_2H_4 VPT2 frequency that is not easily accounted for in the neon and argon matrices is the 850 cm^{-1} frequency of the tribridged isomer, however it is possible that this frequency is blue-shifted to coincide with the 876 cm^{-1} frequency of the dibridged isomer.

Based on the comparison in Table 11 it is clear that neither the dibridged nor tribridged structure is solely responsible for all the Ca_2H_4 peaks observed in the neon and argon matrices. Instead, the most plausible explanation is the dibridged and tribridged structures exist in roughly equal magnitudes and collectively describe all the Ca_2H_4 peaks that have been observed in these matrices. On the other hand, in the krypton matrix there is no conclusive evidence for the tribridged isomer, suggesting that only the dibridged Ca_2H_4 isomer is present. The lack of observation of the tribridged isomer in the krypton matrix is consistent with our understanding that the heavier matrices are more likely to kinetically trap the dibridged isomer.

In the gas phase, interconversion between the dibridged and tribridged isomers would not be hindered from vibrational quenching by the matrix. Therefore at low temperatures we would expect to observe predominantly the tribridged isomer in the gas phase. Only the tribridged isomer of Ca_2H_4 has a permanent dipole moment (10.72 Debye units), thus microwave spectroscopy could be used in the gas phase to distinguish between the tribridged and dibridged Ca_2H_4 isomers.

Table 9 Focal Point Analysis (FPA) of tribridged Ca_2H_4 (M5) relative to dibridged Ca_2H_4 (M4). Energies are in kcal mol^{-1}. The symbol δ indicates an incremental change in energy from the preceding level of theory.

Basis	ΔE_e HF	$+\delta$ MP2	$+\delta$ CCSD	$+\delta$ (T)	$+\delta$ T	$+\delta$ (Q)	ΔE_e Net
DZ	+4.41	−3.19	+0.92	−0.48	−0.07	−0.03	[+1.56]
TZ	+4.07	−5.30	+1.10	−0.78	−0.09	[−0.03]	[−1.03]
QZ	+3.91	−5.80	+1.12	−0.88	[−0.09]	[−0.03]	[−1.77]
5Z	+3.89	−5.98	+1.12	−0.92	[−0.09]	[−0.03]	[−2.01]
CBS	[+3.89]	[−6.17]	[+1.12]	[−0.96]	[−0.09]	[−0.03]	[−2.25]

$$\Delta H_{0K} = \Delta E_{FPA} + \delta_{CR} + \delta_{DBOC} + \delta_{ZPVE} + \delta_{VPT2} \quad = -2.25 - 0.06 + 0.01 + 1.49 - 0.06 = -0.87 \text{ kcal mol}^{-1}$$

Table 10 Fundamental vibrational frequencies of Ca_2H_4 species with anharmonic intensities. Frequencies are given in cm^{-1} and intensities are given in km mol^{-1}.

Species	Frequencies (Intensities)
M4 [HCa(μ_2−H)$_2$CaH]	1276 (a_g, 0), 1258 (b_{3u}, 566), 1056 (b_{3u}, 1486), 1023 (a_g, 0), 952 (b_{1g}, 0), 876 (b_{2u}, 844),
dibridged	496 (b_{1u}, 732), 245 (b_{3g}, 0), 229 (b_{2u}, 661), 207 (a_g, 0), 115 (b_{1u}, 652), 107 (b_{2g}, 0)
M5 [HCa(μ_2−H)$_3$Ca]	1223 (a′, 551), 1168 (a′, 39), 1074 (e, 502 × 2), 850 (a′, 1122),
tribridged	682 (e, 87 × 2), 593 (e, 700 × 2), 255 (a′, 0), 239 (e, 283 × 2)
M6 [Ca(μ_2−H)$_4$Ca]	1099 (a_{1g}, 0), 884 (e_u, 970 × 2), 852 (a_{2u}, 1150), 879 (b_{1g}, 0), 822 (b_{1g}, 0),
tetrabridged	681 (e_u, 687 × 2), 565 (e_g, 0 × 2), 359 (b_{2u}, 0), 305 (a_{1g}, 0)

Table 11 Comparison of experimentally observed Ca_2H_4 bands to VPT2 CCSD(T) frequencies for dibridged and tribridged Ca_2H_4. Frequencies are given in cm^{-1}. The VPT2 frequency closest to the experimentally observed frequency is indicated in bold.

Experiment			M4 dibridged		M5 tribridged	
Ne[a]	Ar[a]	Kr[b]	ν	% Error	ν	% Error
1221			1258	3.0%	**1223**	0.2%
1072	1070		1056	1.5%	**1074**	0.2%
	1057	1044	**1056**	0.1%	1074	1.6%
878	874	870	**876**	0.2%	850	3.2%

[a] Wang and Andrews.[13]
[b] Xiao et al.[12]

4 Conclusions

Three interconvertible isomers were identified for Ca_2H_2. Of these three structures, the dibridged structure was the most enthalpically favored at 0 K, followed by the monobridged structure, and last (surprisingly) the observed linear structure. Despite the thermodynamic favorability of the monobridged and dibridged structures, there is currently only conclusive evidence for the linear Ca_2H_2 structure from the photolysis of calcium in excess hydrogen. We suggest that the linear isomer is intially produced, but is incapable of converting to the more thermodynamically favored constitutional isomers due to vibrational quenching from the matrix. A major goal of future experimental studies is to observe the monobridged and dibridged structures.

Three constitutional isomers for Ca_2H_4 were similarly studied. A near-degeneracy exists between the dibridged and tribridged structures of Ca_2H_4 with the tribridged structure only 0.87 kcal mol^{-1} below the enthalpy of the dibridged structure. Comparison of our VPT2 fundamental frequencies to the unassigned experimental infrared bands from prior studies indicates the coexistence of dibridged and tribridged Ca_2H_4 structures in neon and argon matrices, but only the dibridged structure is observed in a krypton matrix. The results presented in this study should be utilized by future experimental efforts to observe and characterize Ca_2H_2 and Ca_2H_4 species.

Conflicts of interest

There are no conflicts to declare.

Acknowledgments

The authors acknowledge support from the US Department of Energy, Office of Basic Energy Sciences, Computational and Theoretical (CTC) Program and Gas Phase Chemical Physics (GPCP) Program, under Contract No. DE-SC0018412.

Notes and references

1 J. Okuda, D. Mukherjee and D. Schuhknecht, *Angew. Chem. Int. Ed.*, 2018, **57**, 9590–9602.
2 S. Harder and J. Brettar, *Angew. Chem. Int. Ed.*, 2006, **118**, 3554–3558.
3 A. Causero, G. Ballmann, J. Pahl, C. Färber, J. Intemann and S. Harder, *Dalton Trans.*, 2017, **46**, 1822–1831.
4 A. S. Wilson, C. Dinoi, M. S. Hill, M. F. Mahon and L. Maron, *Angew. Chem. Int. Ed.*, 2018, **57**, 15500–15504.
5 X. Shi, G. Qin, Y. Wang, L. Zhao, Z. Liu and J. Cheng, *Angew. Chem. Int. Ed.*, 2019.
6 S. Harder and J. Spielmann, *J. Organomet. Chem.*, 2012, **698**, 7–14.

7 S. Yadav, R. Dixit, M. K. Bisai, K. Vanka and S. S. Sen, *Organometallics*, 2018, **37**, 4576–4584.

8 J. Spielmann and S. Harder, *Eur. J. Inorg. Chem.*, 2008, **2008**, 1480–1486.

9 J.-H. Lim, J.-H. Shim, Y.-S. Lee, J.-Y. Suh, Y. W. Cho and J. Lee, *Int. J. Hydrogen Energ.*, 2010, **35**, 6578–6582.

10 J. Hu, Z. Xiong, G. Wu, P. Chen, K. Murata and K. Sakata, *J Power Sources*, 2006, **159**, 116–119.

11 E. Grube, S. R. Jensen, U. G. Nielsen and T. R. Jensen, *J. Alloy Compd.*, 2019, **770**, 1155–1163.

12 Z. Xiao, R. Hauge and J. Margrave, *High Temp. Sci.*, 1991, **31**, 59–77.

13 X. Wang and L. Andrews, *J. Phys. Chem. A*, 2004, **108**, 11500–11510.

14 M. Kaupp, P. v. R. Schleyer, H. Stoll and H. Preuss, *J. Chem. Phys.*, 1991, **94**, 1360–1366.

15 L. von Szentpály, *J. Phys. Chem. A*, 2002, **106**, 11945–11949.

16 P. Garcia-Fernandez, I. B. Bersuker and J. E. Boggs, *J. Phys. Chem. A*, 2007, **111**, 10409–10415.

17 J. Koput, *J. Phys. Chem. A*, 2005, **109**, 4410–4414.

18 T. J. Tague Jr and L. Andrews, *J. Am. Chem. Soc.*, 1993, **115**, 12111–12116.

19 V. Brites and C. Léonard, *J. Phys. Chem. A*, 2012, **116**, 9484–9489.

20 V. Brites, M. Guitou and C. Léonard, *J. Chem. Phys.*, 2011, **134**, 054314.

21 P. J. Bruna, G. A. Di Labio and J. S. Wright, *J. Phys. Chem.*, 1992, **96**, 6269–6278.

22 T. J. Tague Jr and L. Andrews, *J. Phys. Chem.*, 1994, **98**, 8611–8616.

23 X. Wang and L. Andrews, *J. Phys. Chem. A*, 2004, **108**, 11511–11520.

24 E. Magnusson and S. Petrie, *J. Phys. Chem. A*, 2003, **107**, 6882–6890.

25 M. Kaupp and P. v. R. Schleyer, *J. Am. Chem. Soc.*, 1993, **115**, 11202–11208.

26 D. DeFrees, K. Raghavachari, H. Schlegel, J. Pople and P. v. R. Schleyer, *J. Phys. Chem.*, 1987, **91**, 1857–1864.

27 K. Raghavachari, G. W. Trucks, J. A. Pople and M. Head-Gordon, *Chem. Phys. Lett.*, 1989, **157**, 479–483.

28 J. Koput and K. A. Peterson, *J. Phys. Chem. A*, 2002, **106**, 9595–9599.

29 R. A. Kendall, T. H. Dunning Jr and R. J. Harrison, *J. Chem. Phys.*, 1992, **96**, 6796–6806.

30 I. S. Lim and Y. S. Lee, *J. Chem. Phys.*, 2007, **126**, 104307.

31 I. S. Kerkines and A. Mavridis, *J. Phys. Chem. A*, 2007, **111**, 371–374.

32 A. Shayesteh, S. F. Alavi, M. Rahman and E. Gharib-Nezhad, *Chem. Phys. Lett.*, 2017, **667**, 345–350.

33 H.-J. Werner, P. J. Knowles, G. Knizia, F. R. M. amd M. Schutz, P. Celani, T. Korona, R. Lindh, A. Mitrushenkov, G. Rauhut, K. R. Shamasundar, T. B. Adler, R. D. Amos, A. Bernhardsson, A. Berning, D. L. Cooper, M. J. O. Deegan, A. J. Dobbyn, F. Eckert, E. Goll, C. Hampel, A. Hesselmann, G. Hetzer, T. Hre-nar, G. Jansen, C. Koppl, Y. Liu, A. W. Lloyd, R. A. Mata, A. J. May, S. J. McNicholas, W. Meyer, M. E. Mura, A. Nicklass, D. P. OâĂŹNeill, P. Palmieri, K. Pfluger, R. Pitzer, M. Reiher, T. Shiozaki, H. Stoll, A. J. Stone, R. Tarroni, T. Thorsteinsson, M. Wang, and A. Wolf, *MOLPRO, version 2010.1, a package of ab initio programs*, 2010.

34 J.-Q. Sun and K. Ruedenberg, *J. Chem. Phys.*, 1993, **99**, 5257–5268.

35 F. Eckert and H.-J. Werner, *Theor. Chem. Acc.*, 1998, **100**, 21–30.

36 H. H. Nielsen, *Rev. Mod. Phys.*, 1951, **23**, 90.

37 J. F. Stanton, J. Gauss, L. Cheng, M. E. Harding, D. A. Matthews and P. G. Szalay, *CFOUR, Coupled-Cluster techniques for Computational Chemistry, a quantum-chemical program package*, With contributions from A.A. Auer, R.J. Bartlett, U. Benedikt, C. Berger, D.E. Bernholdt, Y.J. Bomble, O. Christiansen, F. Engel, R. Faber, M. Heckert, O. Heun, M. Hilgenberg, C. Huber, T.-C. Jagau, D. Jonsson, J. Jusélius, T. Kirsch, K. Klein, W.J. Lauderdale, F. Lipparini, T. Metzroth, L.A. Mück, D.P. O'Neill, D.R. Price, E. Prochnow, C. Puzzarini, K. Ruud, F. Schiffmann, W. Schwalbach, C. Simmons, S. Stopkowicz, A. Tajti, J. Vázquez, F. Wang, J.D. Watts and the integral packages MOLECULE (J. Almlöf and P.R. Taylor), PROPS (P.R. Taylor), ABACUS (T. Helgaker, H.J. Aa. Jensen, P. Jørgensen, and J. Olsen), and ECP routines by A. V. Mitin and C. van Wüllen. For the current version, see http://www.cfour.de.

38 M. S. Schuurman, S. R. Muir, W. D. Allen and H. F. Schaefer, *J. Chem. Phys.*, 2004, **120**, 11586–11599.

39 J. M. Gonzales, C. Pak, R. S. Cox, W. D. Allen, H. F. Schaefer, A. G. Császár and G. Tarczay, *Chem. Eur. J.*, 2003, **9**, 2173–2192.

40 A. G. Csaszar, W. D. Allen and H. F. Schaefer, *J. Chem. Phys.*, 1998, **108**, 9751–9764.

41 A. L. East and W. D. Allen, *J. Chem. Phys.*, 1993, **99**, 4638–4650.

42 D. Feller, *J. Chem. Phys.*, 1992, **96**, 6104–6114.

43 T. Helgaker, W. Klopper, H. Koch and J. Noga, *J. Chem. Phys.*, 1997, **106**, 9639–9646.

44 M. Kállay, Z. Rolik, J. Csontos, I. Ladjánszki, L. Szegedy, B. Ladóczki, G. Samu, K. Petrov, M. Farkas, P. Nagy *et al.*, *See also: http://www.mrcc.hu*, 2015.

45 S. Stopkowicz and J. Gauss, *J. Chem. Phys.*, 2008, **129**, 164119.

46 H. Sellers and P. Pulay, *Chem. Phys. Lett.*, 1984, **103**, 463–465.

47 N. C. Handy, Y. Yamaguchi and H. F. Schaefer, *J. Chem. Phys.*, 1986, **84**, 4481–4484.

48 J. M. Merritt, V. E. Bondybey and M. C. Heaven, *Science*, 2009, **324**, 1548–1551.

49 P. Li, W. Xie and K. Tang, *J. Chem. Phys.*, 2010, **133**, 084308.

50 W. J. Balfour and R. F. Whitlock, *Can. J. Phys.*, 1975, **53**, 472–485.

51 J. C. Miller, B. S. Ault and L. Andrews, *J. Chem. Phys.*, 1977, **67**, 2478–2487.

52 X. Biquard, O. Sublemontier, J. Berlande, M. Gaveau, J. Mestdagh and J. Visticot, *J. Chem. Phys.*, 1995, **103**, 957–965.

53 J. Francis Jr and S. Webber, *J. Chem. Phys.*, 1972, **56**, 5879–5886.

54 C. Vidal, *J. Chem. Phys.*, 1980, **72**, 1864.

55 O. Allard, A. Pashov, H. Knöckel and E. Tiemann, *Phys. Rev. A*, 2002, **66**, 042503.

56 O. Allard, C. Samuelis, A. Pashov, H. Knöckel and E. Tiemann, *Eur. Phys. J. D*, 2003, **26**, 155–164.

57 D.-D. Yang and F. Wang, *Theor. Chem. Acc.*, 2012, **131**, 1117.

58 K. Patkowski, R. Podeszwa and K. Szalewicz, 2007, **111**, 12822–12838.

59 N. S. Mosyagin, A. N. Petrov, A. V. Titov and A. V. Zaitsevskii, *Int. J. Quant. Chem.*, 2013, **113**, 2277–2281.

60 D. Petitprez, B. Lemoine, C. Demuynck, J. Destombes and B. Macke, *J. Chem. Phys.*, 1989, **91**, 4462–4467.

61 K.-P. Huber and G. Herzberg, *Molecular Spectra and Molecular Structure: IV. Constants of Diatomic Molecules*, Springer Science & Business Media, 2013.

62 J. Chen and T. C. Steimle, *J. Chem. Phys.*, 2008, **128**, 144312.

63 T. Hrenar, H.-J. Werner and G. Rauhut, *Phys. Chem. Chem. Phys.*, 2005, **7**, 3123–3125.

64 B. Bussery-Honvault and R. Moszynski, *Mol. Phys.*, 2006, **104**, 2387–2402.

65 D. E. Woon and T. H. Dunning Jr, *J. Chem. Phys.*, 1994, **100**, 2975–2988.

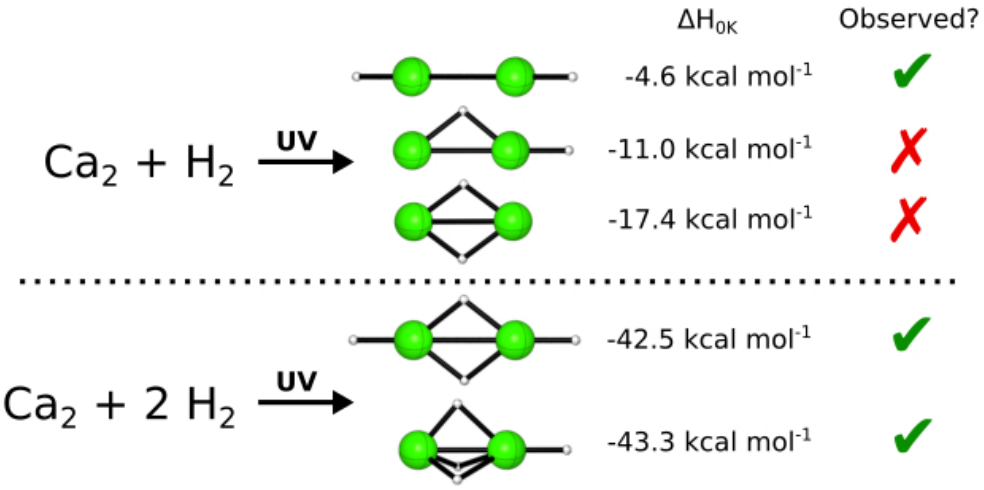
ΔH0K
Observed?
Ca2 + H2
UV
-4.6 kcal mol-1
-11.0 kcal mol-1
-17.4 kcal mol-1
Ca2 + 2 H2
UV
-42.5 kcal mol-1
-43.3 kcal mol-1